Acknowledgments

Table of Contents

List of Tables ..... **iv**

List of Figures ..... **v**

Chapter 1: Introduction **1**

Chapter 2: Experimental Methods **2**

2.1 First Optics Enclosure 4

2.1.1 Bremsstrahlung Collimator 4

2.1.2 Beam-splitting Mirror 5

2.2 Second Optics Enclosure 7

2.2.1 Septum Mask 7

2.3 Coherent Diffraction Hutch 8

2.3.1 Rollerblade Slits 9

2.3.2 Kirkpatrick-Baez Mirrors 10

2.3.3 Diffractometer 11

2.3.4 Sample 13

2.3.5 Experiment 13

2.3.6 Reconstruction 17

Chapter 3: Results **22**

Chapter 4: Analysis **23**

References **25**

List of Tables

Table 2.1: Angle phi as a function of inclination of the sample (while theta = 0˚)..... 14

Table 2.2: List of parameters required for the reconstruction process along with how to obtain the values..... 21

List of Figures

Figure 2.1: Floor map of Sector 34 at the APS 3
Figure 2.2: Bremsstrahlung collimator along with the supplemental lead blocks 4
Figure 2.3: Beam-splitting Mirror with Nitrogen feed 5
Figure 2.4: Beam sharing schematic 6
Figure 2.5: Distance between the two beams as it reaches the Septum Mask 7
Figure 2.6: View through the window of the Septum Mask 7
Figure 2.7: Rollerblade slits. The horizontal Molybdenum slits can be seen clearly while the vertical slits are covered by the holder. 9
Figure 2.8: Rollerblade slits. a) Slits allowing full X-ray beam through. b) Slits slightly rotated to allow only a fraction of the beam through 10
Figure 2.9: Schematic of a Kirkpatrick Baez mirror 10
Figure 2.10: Mirror positioning 11
Figure 2.11: Different diffractometer angles. a) Top view of the diffractometer. b) Side view of the diffractometer 12
Figure 2.12: Top view of the sample holder with the sample 12
Figure 2.13: Image showing the sample holder, sample stage, photomultiplier tube (PMT), overhead camera and KB mirror 13
Figure 2.14: Motor controls - Rollerblade slits 14
Figure 2.15: Example of an expected diffraction pattern 15
Figure 2.16: a) Block diagram of the Error Reduction (ER) algorithm; b) block diagram of the system for the Hybrid Input-Output (HIO) algorithm 17
Figure 2.17: Diffraction pattern of a typical nanowire shown at frame = 22 (top left), 34 (top right), 49 (bottom left) and 63 (bottom right) – 'Aliens' are circled 20

Chapter 1: Introduction

- Growth of nanowires - VLS
- Traditional optical microscope – best optics unable to see at nanometer level
- SEM – cannot get structural data such as strain
- CXD – able to reconstruct high resolution nano-sized objects and also gain structural data
- A bit about the APS facility
- Synchrotron radiation – how it is produced
- Bremsstrahlung radiation – how it is produced
- The need to contain both types of x-ray radiation (safety reasons)
- Algorithms – Error Reduction, Hybrid Input Ouput (At the moment, this section is in 2.3.6 – Reconstruction but I'm not sure if I should talk about the algorithms here in the Introduction?)

Chapter 2: Experimental Methods

The experiments were performed at the Advanced Photon Source located at the Argonne National Laboratory in Chicago, US. The Advanced Photon Source (APS) is a large synchrotron x-ray facility. Within the APS, the experiments were performed at the Coherent Diffraction station found within Sector 34 of the APS, known as 34-ID-C (see Figure 2.1).

The X-rays are generated via an Undulator, with the beam splitting mirror placed 29m away from it. The beam splitting mirror is used here to produce two separate beams, known as the white beam and the pink beam (white beam with higher energies removed)[1]. The pink beam allows for the Coherent X-ray Diffraction experiments performed at Sector 34-ID-C, whereas the white beam is used for Microfocus Diffraction experiments performed at the neighbouring Sector 34-ID-E. The details for the Microfocus Diffraction are not relevant for the purposes of this report.

Sector 34 is split into five separate hutches where the first hutch is known as Sector 34-ID-A (also known as First Optics Enclosure). This is where the beam enters from the undulator to Sector 34 separated by a concrete wall. The beam-splitting mirror is located in this hutch. The second hutch is known as Sector 34-ID-B (also known as Second Optics Enclosure), and this is where the two separate beams have their own pipes. The third hutch, known as Sector 34-ID-C (also known as Coherent Diffraction Hutch) is where the coherent x-ray diffraction experiments are performed and is the first of the two experimental hutches. The fourth and fifth hutches known as Sector 34-ID-D (or Third Optics Enclosure) and Sector 34-ID-E (or Microfocus Diffraction Hutch) relate to the microfocus diffraction experiments where the white beam is used. All five hutches have lead doors covered by steel to prevent x-rays from exiting the hutch.

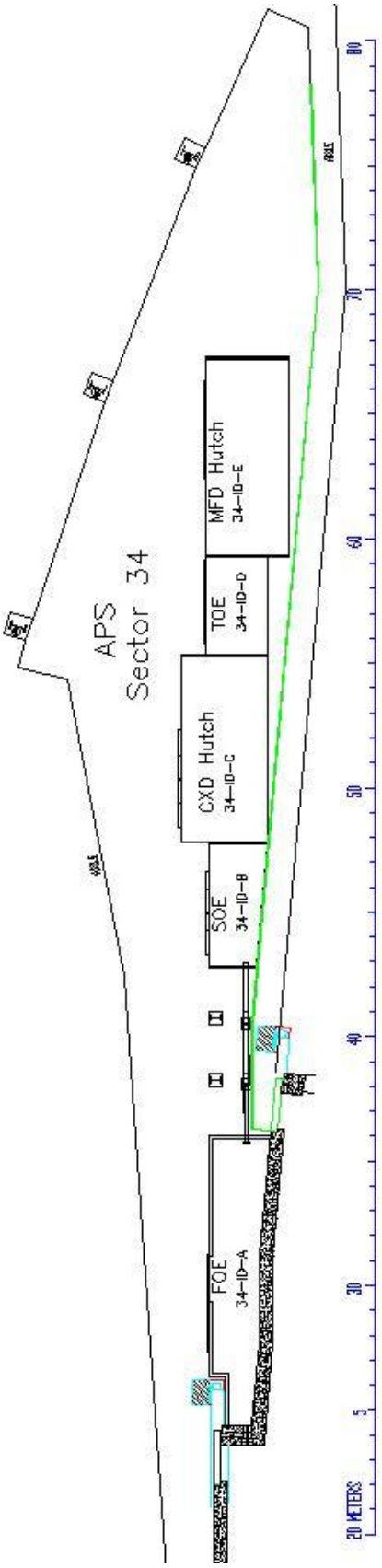

Figure 2.1: Floor map of Sector 34 at the APS

2.1 First Optics Enclosure

Due to the high flux of photons emerging from the source, it is vital to cool down the x-ray beam whenever it comes into contact with a component; hence all components are either water or nitrogen cooled.

Before the full white beam reaches the beam splitting mirror, the beam travels through several components to ensure the mirror is not damaged by the heat. Firstly, the beam travels through a Front End Mask which cuts the beam down to 4.5mm horizontally by 4.5mm vertically. The Front End Mask is required to protect the components that follow from a missteered beam. The next component is a thermal mask which reduces the beam further down to 4mm horizontally by 2mm vertically to ensure that the subsequent components are protected by the extreme heat flux. It is vital to cool the mask to avoid any damage to the components due to excessive heat, hence the mask is water cooled with continuous water running through the component.

2.1.1 Bremsstrahlung Collimator

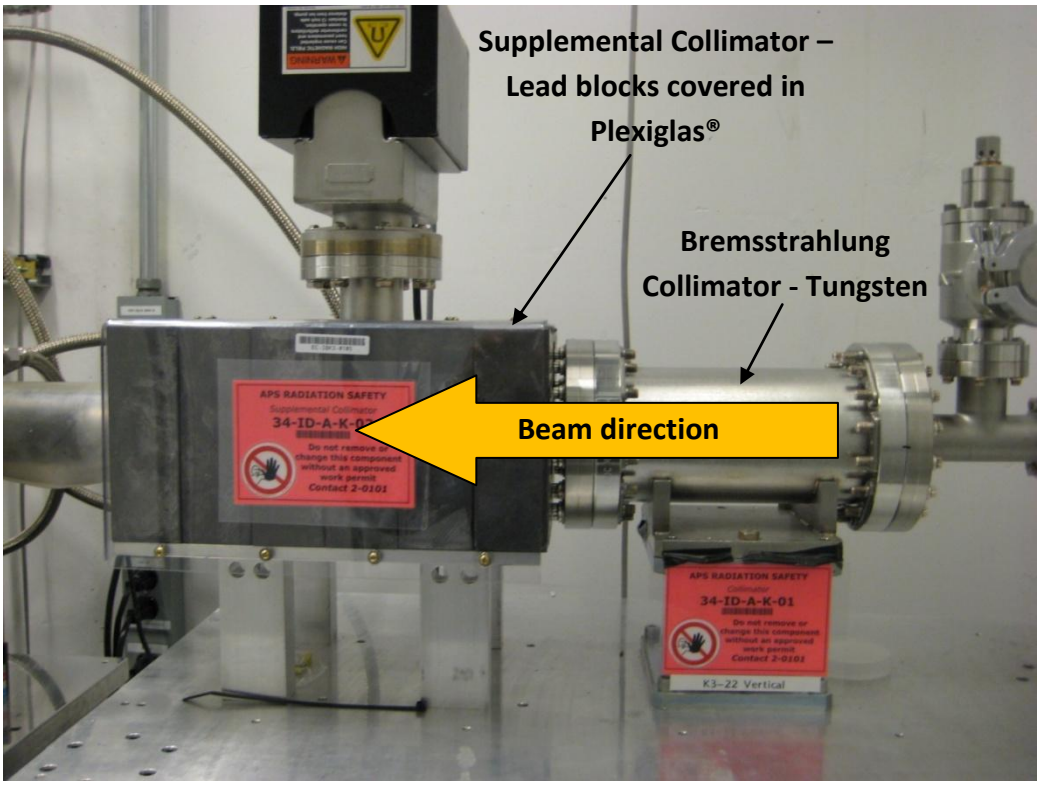

Figure 2.2: Bremsstrahlung collimator along with the supplemental lead blocks

The next component to follow is the Bremsstrahlung Collimator which is a tungsten cylinder of 100mm diameter with a 6mm diameter aperture in the middle through which the x-ray beam travels. The collimator blocks out any unwanted Bremsstrahlung

radiation, although the collimator itself is not enough to shield the Bremsstrahlung radiation in the horizontal direction. Hence two sets of lead blocks (100mm wide by 140mm high) are placed on each side of the beam as it leaves the collimator (see Figure 2.2). Further slits are used, known as pre-mirror slits, to reduce the beam dimensions further.

2.1.2 Beam-splitting Mirror

The Beam-splitting Mirror is the subsequent component following the slits. The mirror consists of a polished Silicon (111) substrate (30mm wide by 30mm high by 220mm long). The 30mm height of the substrate is split into three separate parts: a 10mm rhodium strip, a 10mm platinum strip and the remaining part is kept as bare silicon. This opens up three separate options when choosing the mirror surface; rhodium, platinum and silicon. The surface used in the experiments herein is the bare silicon surface.

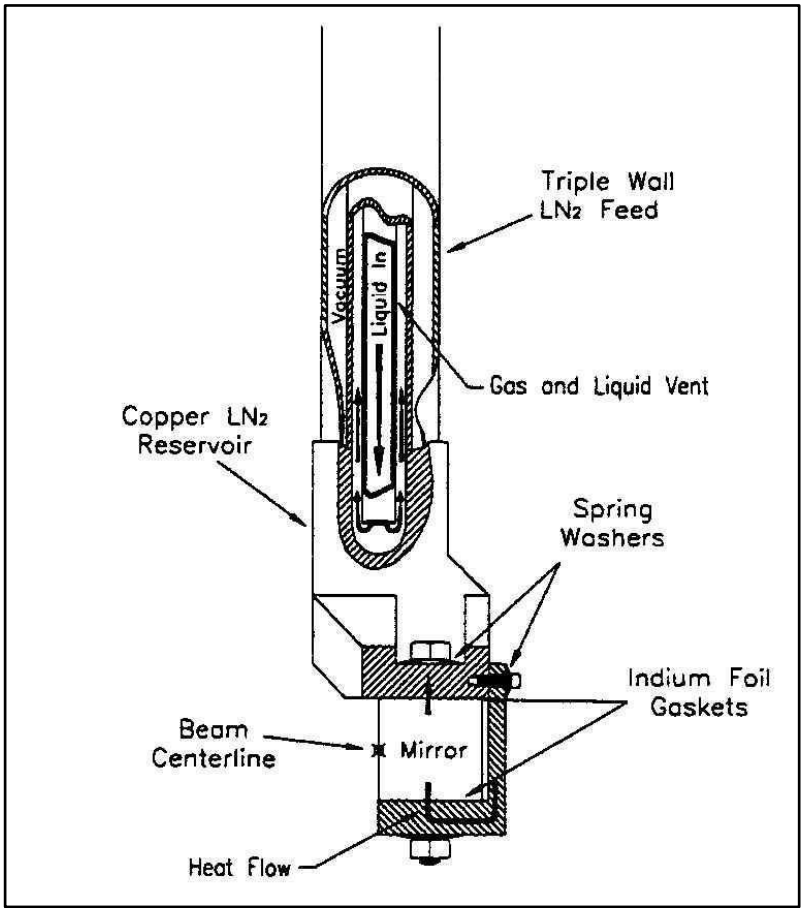

Figure 2.3: Beam-splitting Mirror with Nitrogen feed[3]

The beam-splitting mirror faces a very high heat flux and so to prevent it from deforming, the mirror is cooled cryogenically using liquid nitrogen. *"If we were to use water cooling on a mirror with a similar cross-section to ours, we would estimate a "thermal bump" on a 1mm wide heated spot to induce large slope errors on the order of 0.25mrad. Since the coefficient of thermal expansion for silicon below 130K is less than a fifth of its value at room temperature, and the heat conductivity is much higher,*

our mirror will be cryogenically cooled to minimize these heat-induced distortions by at least a factor of 20"[2] The arrangement of the mirror with the nitrogen feed can be seen in Figure 2.3.

The liquid nitrogen is gravity fed into the system where it comes into contact with the copper mirror holder. It is vital for the mirror to be stable due to the accuracy required from the mirror arrangement. Hence, the mirror is held firmly in place to the copper mirror holder using four ¼" bolts. *'Bellville spring washers are used on each bolt to evenly distribute the clamping force and allow for differential expansion between the stainless steel bolts and the silicon as the assembly is cooled.'*[3] Indium foil gaskets are used to improve thermal conductivity between the copper holder and the silicon mirror.

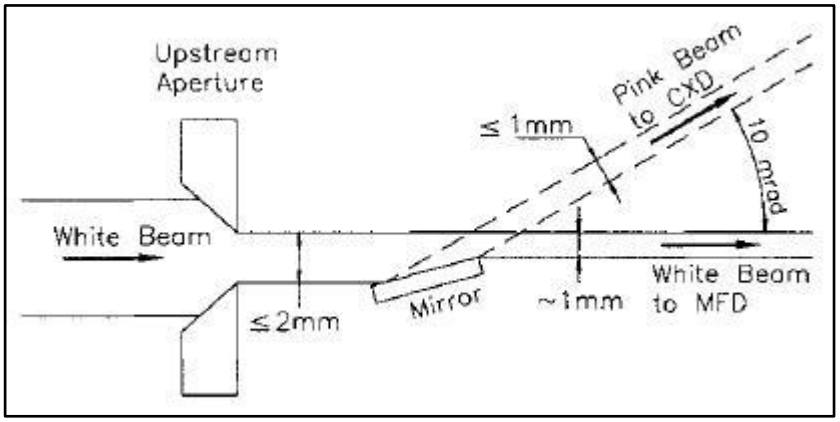

Figure 2.4: Beam sharing schematic[2]

The incoming white beam is split into two using the beam-splitting mirror as depicted in Figure 2.4. The mirror is placed such that half of the incoming white beam is reflected off the mirror and is known as the pink beam, while the other half passes through without any interaction with the mirror and hence remains as the white beam. The two parts of the beam are both 1mm horizontally and 1.5mm vertically immediately after the mirror. The mirror is placed at an angle of 5mrad to the horizontal which results in the pink beam diverting at an angle of 10mrad from the horizontal. Due to the two beams being in very close proximity, they coexist in the same pipe until the distance between the two is great enough to allow for separate pipes.

The next component in place is the first white beam transport which has a diameter of 200mm covered by 12mm of lead. The white beam transport is essentially a pipe made of stainless steel so as to minimise the loss of pressure. The 12mm lead ensures that any radiation leakage due to scattering from molecules of air within the transport is blocked.

A pump station is located prior to the end of the First Optics Enclosure, which maintains the ultra high vacuum inside the components and the transport. The white beam transport runs through the hutch wall and continues on for about 6.5 metres before it enters the Second Optics Enclosure.

2.2 Second Optics Enclosure

2.2.1 Septum Mask

The first component found in this hutch is the Septum Mask which essentially allows the two branches of the beam to have their own pipes. The distance between the beam-splitting mirror and the septum mask is approximately 13 meters. By simple calculation, as shown in Figure 2.5, it can be seen that the horizontal gap between the two beams at this point is 130mm and hence enough to allow two separate pipes for the two beams.

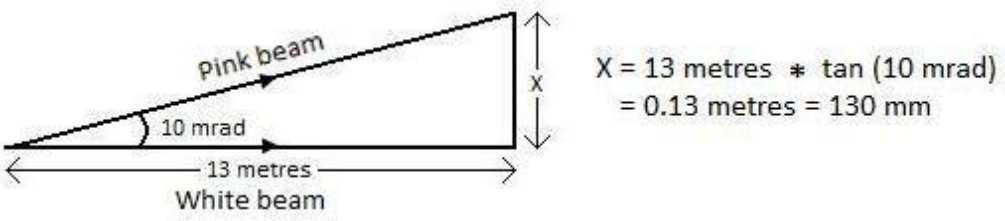

Figure 2.5: Distance between the two beams as it reaches the Septum Mask

The septum mask is made such that it can *'dissipate the full power of the pink beam whenever the mirror is missteered'*[4]. The faces inside the mask are made of Glidcop® (dispersion strengthened Copper with Aluminium Oxide)[5], which are water cooled in the case of any beam missteerings. The mask also consists of a window where the pink and white beam apertures are visible for visual examination of the beam (see Figure 2.6). The Glidcop surface, as well as being able to withstand the full heat of a pink beam, also acts as a fluorescence material hence visually allowing one to steer the pink beam into its aperture.

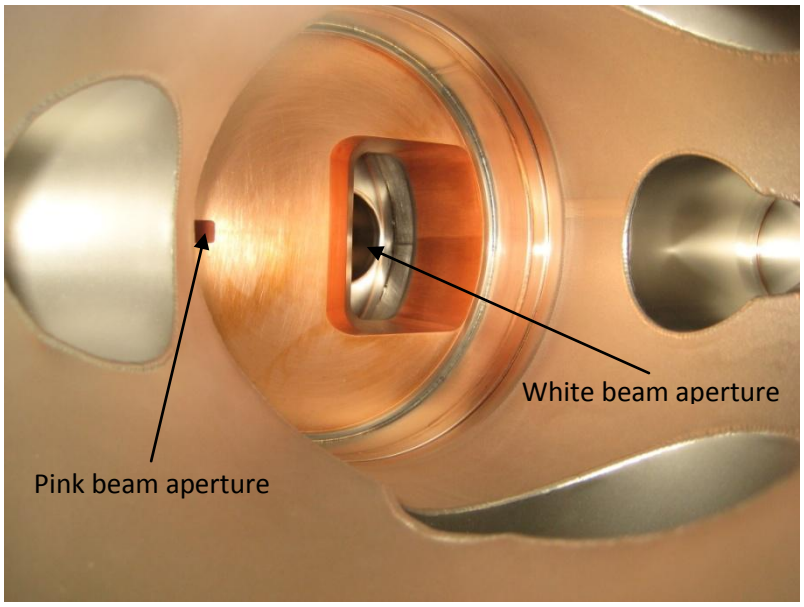

Figure 2.6: View through the window of the Septum Mask

As the pink beam is now separated from the white beam, focus will be placed solely on the pink beam as it is used for the coherent x-ray diffraction experiments. As the beam-splitting mirror is invisible to Bremsstrahlung radiation, the pink beam does not consist of a Bremsstrahlung component, hence further Bremsstrahlung collimators are not required for the pink beam but are only required for the white beam. The white beam follows the pink beam into the Coherent Diffraction Hutch but then carries on further into the Third Optics Enclosure and finally into the second experimental hutch, Microfocus Diffraction Hutch, where it terminates.

The next component in line is a Beryllium window which acts as a separator for the two vacuum systems either side of it. Beryllium windows allow x-rays to pass through it yet maintain the vacuum within the system. This is particularly important once the pink beam reaches the Coherent Diffraction Hutch as discussed in Section.2.3.

A pink beam position monitor is the next component in line which consists of two diamond blades placed above and below the pink beam. Diamond blades are used due to their *'superior thermophysical properties, such as high thermal conductivity, a low thermal expansion coefficient, and good mechanical strength and stiffness under heat'*[6]. The beam position monitor works by feeding back the horizontal position to the piezo positioner of the beam-splitting mirror.[4]

The final two components in the Second Optics Enclosure that are related to the pink beam are the monochromator and the pink beam shutter. The monochromator .....need to email prof robinson about this... silicon or diamond? Also beam splitting mirror.....which face used? Silicon? Rhodium? Platinum? The monochromator article suggests platinum was used.

The pink beam shutter consists of water cooled oxygen-free high-conductivity copper (OFHC) and Glidcop® copper blocks which absorb the pink beam (synchrotron radiation)[7]. The shutter is made fail-safe so in the case of any electrical, mechanical or communication failure, the shutter is closed and will remain closed[8]. The shutter also consists of two 35mm thick tungsten blocks which allow safe access to the Coherent Diffraction Hutch. The total maximum heat load accepted by the shutter is 600 Watts, whereas the worst case power level expected for the pink beam is 165 Watts[4].

2.3 Coherent Diffraction Hutch

This is where the coherent x-ray diffraction experiments take place. The following vital components are located in this hutch:

- Rollerblade Slits
- Kirkpatrick-Baez Mirrors
- Diffractometer

2.3.1 Rollerblade Slits

The first vital component here is the rollerblade slits. The slit consists of two polished molybdenum rods which are computer controlled externally from outside the hutch. Figure 2.7 shows the roller-blade slits as seen from the window of the ultra-high vacuum chamber that it is contained in. Each slit is controlled by two micrometers, one being the position micrometer and other being the gap micrometer which determines the gap between the two Molybdenum rods.

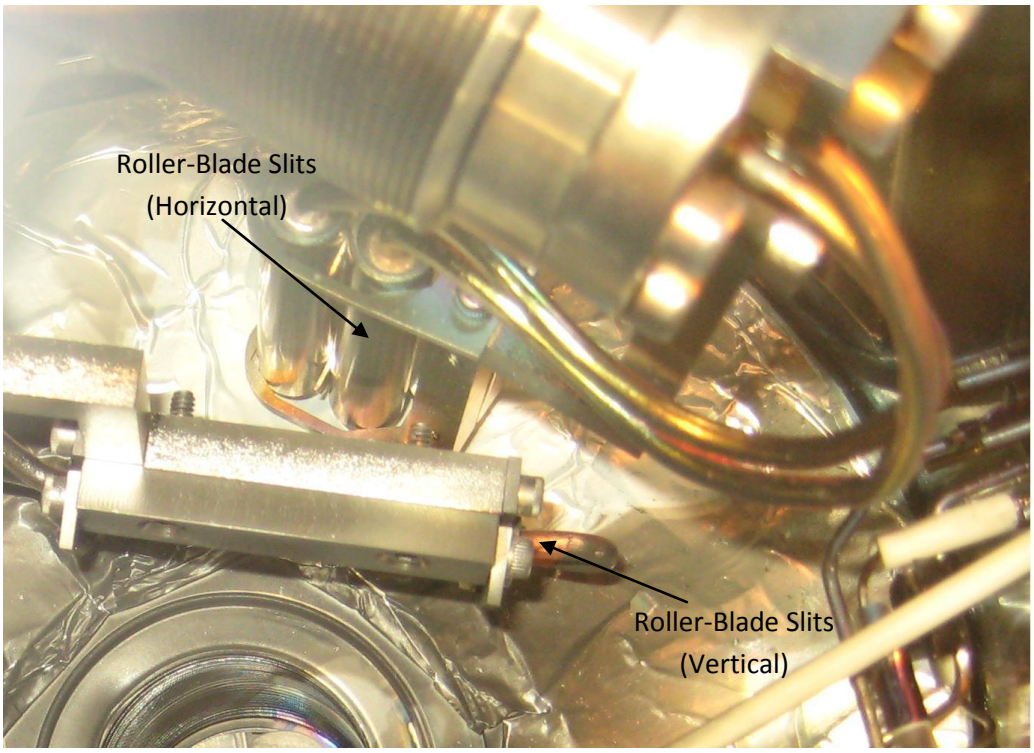

Figure 2.7: Rollerblade slits. The horizontal Molybdenum slits can be seen clearly while the vertical slits are covered by the holder.

The slits work via a rotation mechanism whereby the axis of rotation is directly between and parallel to the two rods (see Figure 2.8). By rotating about this axis, one can vary the gap between the two rods and hence doing this horizontally and vertically, gives a pin point of x-ray radiation. The gap micrometer of the horizontal slit is calibrated such that moving 0.0420 mm corresponds to a change in the horizontal gap by 1 µm. Similarly for the vertical slit, moving 0.0280 mm corresponds to a change in the vertical gap by 1 µm. The horizontal and vertical gaps used for the experiments are as follows:

- Horizontal = 1.0500 mm which corresponds to a horizontal gap of 25 µm
- Vertical = 1.4000 mm which corresponds to a vertical gap of 50 µm

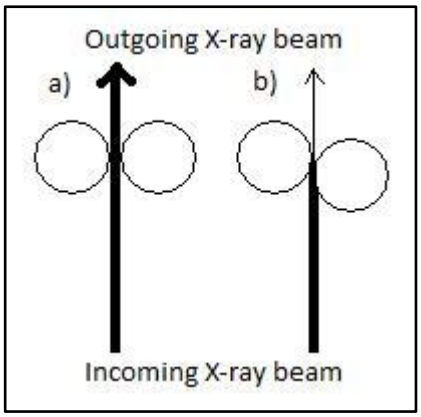

Figure 2.8: Rollerblade slits. a) Slits allowing full X-ray beam through. b) Slits slightly rotated to allow only a fraction of the beam through

2.3.2 Kirkpatrick-Baez Mirrors

The next vital components in line are the horizontally and vertically placed Kirkpatrick-Baez (KB) mirrors which are trapezoidal silicon mirrors. The main purpose of the KB mirrors is to focus the x-ray beam down to approximately 1 µm by 1 µm. The reason the mirrors are trapezoidal is so that they can be bent to elliptical shapes. Figure 2.9 shows the arrangement of the KB mirror along with the force inducing holder which bends the mirror into an elliptical shape.

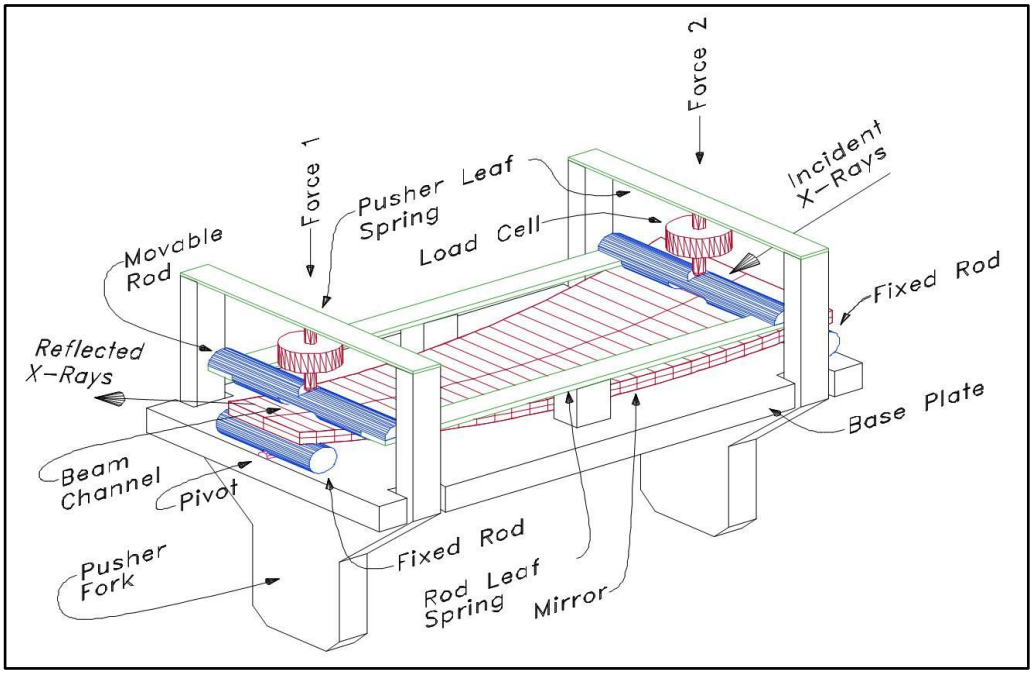

Figure 2.9: Schematic of a Kirkpatrick Baez mirror[9]

The concept of using mirrors to focus x-rays was first suggested by Kirkpatrick and Baez in 1948[10]. The technique was further developed by many others and such mirrors are now named after Kirkpatrick and Baez. Initially the mirror is an extremely flat surface but using the mechanism shown in Figure 2.9, the mirror is bent into an elliptical shape

off which the incoming x-rays graze off. The two separate forces on either side of the mirror allow flexibility in the shaping of the mirror and hence the end x-ray spot size. The two separate horizontal and vertical mirrors allow one to vary the magnification of the horizontal and vertical components of the beam independently of each other.

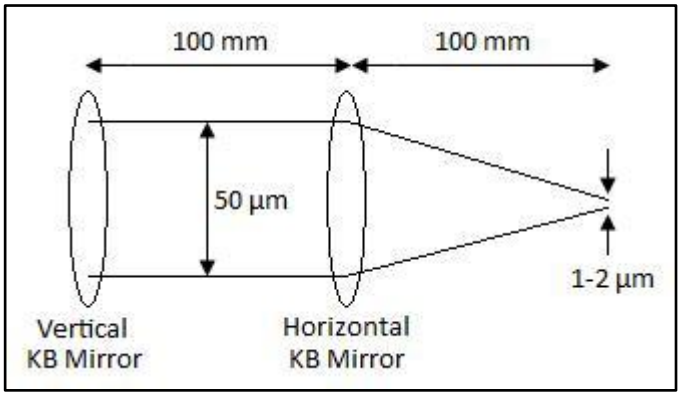

Figure 2.10: Mirror positioning

The positioning of the two mirrors is shown in Figure 2.10. The two mirrors are separated by a gap of 100mm, while the horizontal KB mirror is also placed 100mm away from the sample, where the beam size is focused down to 1-2 µm.

2.3.3 Diffractometer

The Diffractometer is the next vital component in line. This is where the sample and detector are located. Due to the close proximity of the white beam transport running through the Coherent Diffraction Hutch, through to the Third Optics Enclosure, the diffractometer is designed such that the permanent presence of the white beam transport does not compromise the functionality of the diffractometer.

Figure 2.11 shows the different angles involved with the orientation of the sample and detector. The sample is controlled by three angles: theta, phi and chi. The sample may also be moved in the three translational directions: x, y and z. Theta rotates the sample about its centre, while phi tilts the sample in the y direction and chi tilts the sample in the x direction. As x and y are relative to the value of theta, y is defined as being parallel to the beam when theta is 0˚ and perpendicular to the beam when theta is 90˚. Similarly x is perpendicular to the beam when theta is 0˚ and parallel when theta is 90˚. The sample stage may be controlled via two computers: an external computer found outside the Coherent Diffraction Hutch and an internal computer located inside the hutch.

The detector arm is controlled by three separate angles: delta, gamma and nu. Delta and gamma are as shown in Figure 2.11, where delta moves the detector arm horizontally, while gamma moves the detector arm vertically. Nu, not shown in Figure 2.11, rotates the detector about its centre, but is not as vital as gamma and delta and hence is not utilised much during the experiments.

The detector used in the experiments is a 100 kHz (16 bits) Charge Coupled Device (CCD), which along with an Analogue to Digital Converter (ADC) record the number of photons shining on it and convert this to an electrical signal.

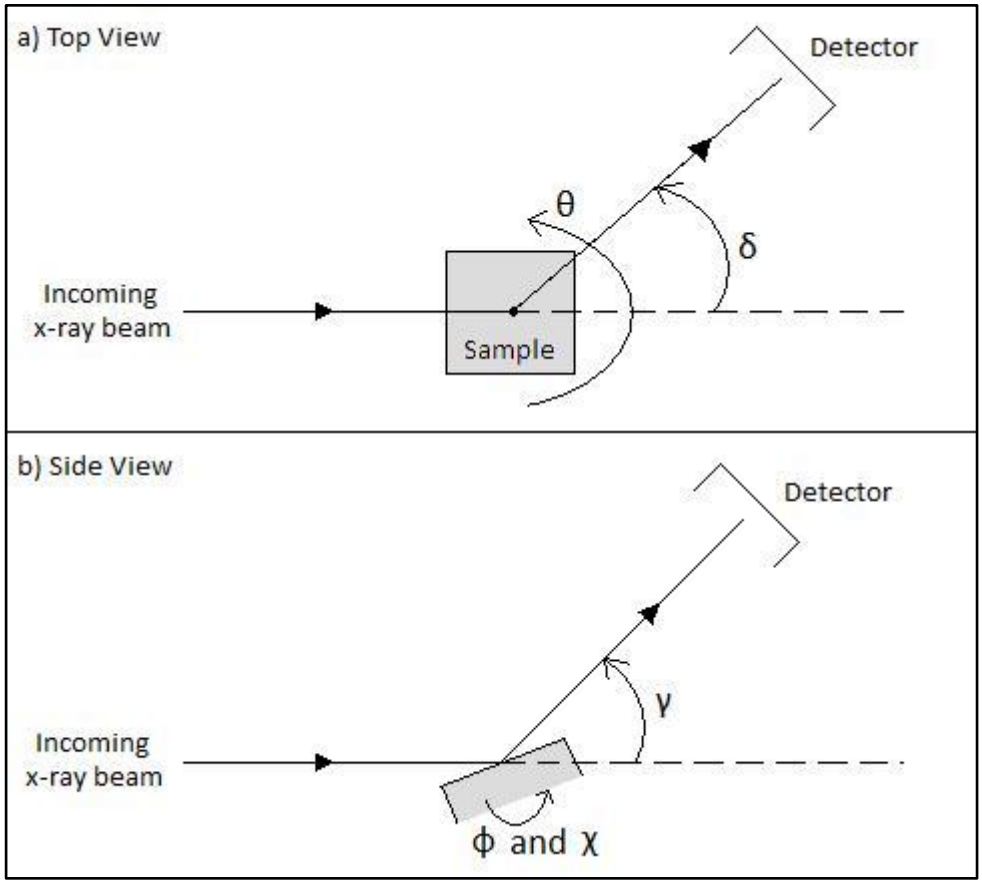

Figure 2.11: Different diffractometer angles. a) Top view of the diffractometer. b) Side view of the diffractometer

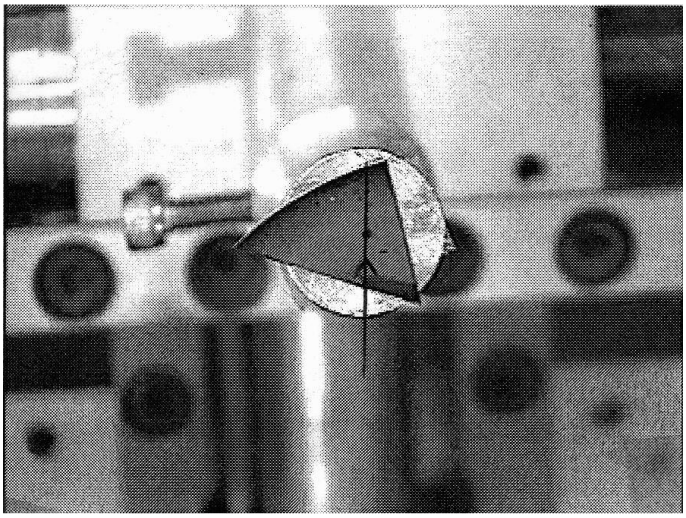

Figure 2.12: Top view of the sample holder with the sample

The other useful component in this hutch is a camera found directly above the sample, which is connected to a television screen found outside of the hutch. This live camera

feed allows one to control which part of the sample the beam makes impact with. The beam centre is marked on the television screen during the calibration process. Figure 2.12 shows the sample as viewed from this camera. The sample is approximately a 1cm triangular piece of Silicon substrate onto which the Indium Phosphide nanowires are grown.

Figure 2.13 shows the arrangement of the sample stage, KB mirrors, photomultiplier tube (PMT) and the overhead camera. The close proximity of the KB mirrors and the sample is evident in this image.

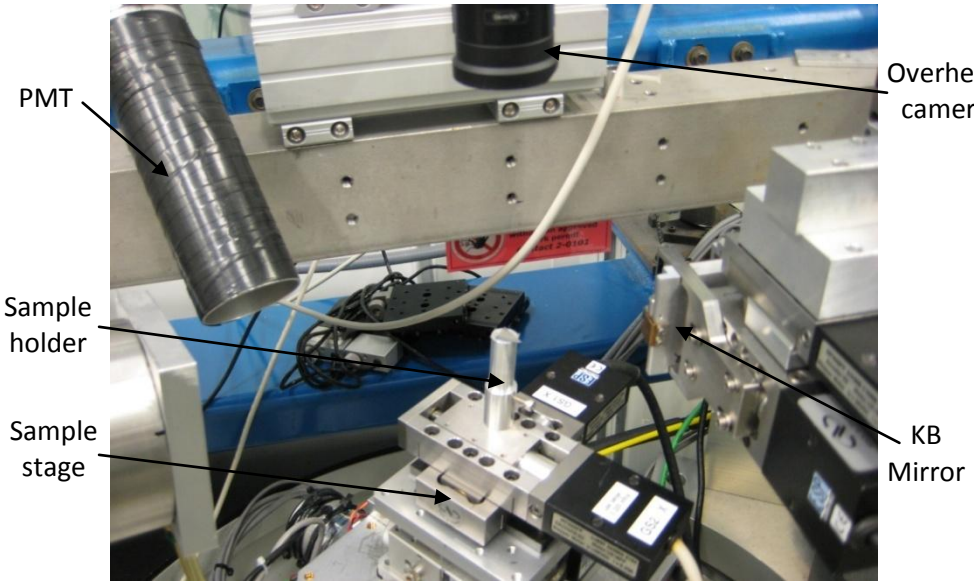

Figure 2.13: Image showing the sample holder, sample stage, photomultiplier tube (PMT), overhead camera and KB mirror.

2.3.4 Sample

The Indium Phosphide samples (InP #4 and InP #5) were grown by Suneel Kodambaka and Robyn Woo at the University of California Los Angeles (UCLA)[11]. *"The InP (Indium Phosphide) nanowires were grown via VLS (Vacuum-Liquid-Solid) using Indium catalysts. It's a two-step growth process. First, we deposited In (Indium) droplets by feeding 1 × 10^{-5} mol/min of TMIn (trimethylindium) for 30 sec at 350˚C. Then, InP (nanowires) were grown by feeding 1 × 10^{-5} mol/min of TMIn and 8 × 10^{-4} mol/min of TBP (tertiarybutylphosphine) for 15 min at the same temperature."*[12]

2.3.5 Experiment

Before the diffraction experiments can be carried out, the apparatus needs to be calibrated. The calibration process has various steps as outlined here. Firstly, the rollerblade slits need to be adjusted to the correct beam size. A beam size of 25 µm (horizontally) by 50 µm (vertically) will be used. This is done by using the software shown in Figure 2.14, which is found on both the internal and external computers.

The KB mirrors are next focused to give a vertical focus of 2.1 µm and a horizontal focus of 2.8 µm. The focusing is done by using a sharp pin in place of the sample to align the beam and then using crosshairs to focus it. The next step is to replace the crosshairs with the sample (InP #4), which is positioned in place on the sample holder as shown in Figure 2.13. The sample has to be held in place firmly to prevent any movements of the sample due to environmental conditions or due to the high flux of the x-ray beam itself, hence sticky back tape is used to hold the sample in place.

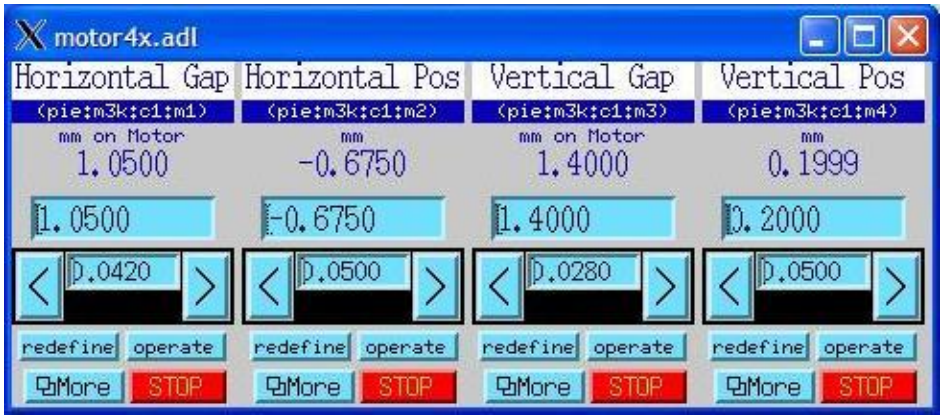

Figure 2.14: Motor controls - Rollerblade slits

The next step is to adjust the chi and phi angles along with the z value. The height of the sample holder, z, is varied until a beam can be seen on the output of the CCD camera. Next step is to calibrate phi such that the beam doesn't reflect off the surface of the sample, but slides over it. This is done by keeping theta at 0˚ and varying phi until a reflection can be seen on the screen as well as the actual x-ray spot. At this point, the x-ray beam is partially reflecting off the surface and partially going straight through to the CCD camera. As we require grazing off the surface of the sample, the phi angle is varied more until the two spots, the reflection spot and the actual beam spot, as seen on the CCD camera, become one. At this point, the x-ray beam is just grazing off the sample. Similarly, to calibrate the chi value, the sample first needs to be rotated 90˚, which is done by changing theta to 90˚. The same procedure as for calibrating phi is carried out for the calibration of chi. Theta is changed back to 0˚.

The next step is to set the lattice constant of Indium Phosphide (a_{InP} = 5.87Å) using the terminal window in the external computer. Due to silicon Bragg peaks interfering with the (1, 1, -1) indium phosphide Bragg peaks, it was decided that we will look at the (5/3, -1/3, -1/3) indium phosphide Bragg peaks. Once this is set, the sample is inclined to a small angle of 5˚, so the x-ray beam reflects off the sample. Table 2.1 shows how the sample holder needs to be tilted, via the angle phi, as a function of the inclination angle.

Inclination, α	Phi, ϕ
0˚	0.66˚ (for example)
5˚	0.66˚ - 5˚ = -4.34˚

Table 2.1: Angle phi as a function of inclination of the sample (while theta = 0˚)

The two-theta (Bragg) angle for the (5/3, -1/3, -1/3) peak is determined by typing the following command in the terminal: “ca 5/3 -1/3 -1/3”. This also outputs the delta and gamma angles (detector angles) to give the desired two-theta value. Once the detector has been moved to the desired two-theta value, the CCD camera output, visible on one of the external computers, shows strong Bragg peaks. To avoid damage to the CCD camera from these extremely strong (5/3, -1/3, -1/3) Bragg peaks, the detector is moved slightly downwards and away from the main Bragg peaks where the search for Indium Phosphide nanowires can begin.

The process of searching for InP nanowires is outlined below:

1) The two-theta value is kept constant by keeping the delta and gamma angles constant
2) Manual search in either x or y directions is carried out
3) Once an interesting diffraction pattern is seen on the CCD output, it is centralized on the screen using the two detector angles, delta and gamma

Interesting diffraction pattern compromises of a bulk in the centre with fringes seen on either side of it at an angle (see Figure 2.15).

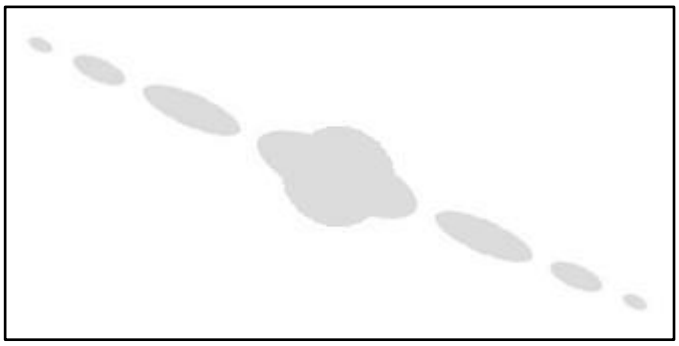

Figure 2.15: Example of an expected diffraction pattern

Once a potentially good diffraction pattern is found, the pattern needs to be optimised by varying the x, y and theta values to obtain the most intense pattern. (The brightest part of the pattern is the central part, which is discussed further in the Analysis section). Theta is now reduced until the pattern disappears and then increased until the pattern becomes bright and then disappears once again. This is to get an idea of the variation in theta before the pattern disappears.

Once the variation in theta is noted down, the pattern is brought back to its most intense state which is approximately in the middle, by reducing theta once more. At this position, a brief scan of 1 second exposure time is carried out to obtain the intensity of the centre of the pattern. The CCD camera is capable of withstanding intensities of up to 2^{16} (or 65,536) photon counts per pixel (This is the reason why we have moved away from the main Bragg peaks as the intensities there are well in excess of 65,000 photon counts per pixel and therefore would burn a hole in the CCD camera). Hence to optimise the results, central intensity of the pattern of approximately 65,000 photon counts per pixel is sought. This is achieved by adjusting

the exposure time accordingly. For example, if the above 1 second exposure time resulted in a central intensity of 20,000 photon counts per pixel, then the an exposure time of 3 seconds would make the best use of the available 16 bit CCD camera and also obtain optimum results from the scan.

A full scan is now appropriate and is carried out by following the subsequent steps:

1) Make a note of the theta range where the pattern is visible (this task was carried out earlier).
2) On the terminal window, the scan may be initiated via one of the following two ways:
    a. Using the *lineup ('lup')* function where the function is used as follows:
        - *'lup th -0.3 0.3 30 -10'*
        - The *'th'* lets the system know that we want to vary theta
        - *'-0.3'* and *'0.3'* refer to how many degrees to move in the negative and positive directions from the current position, respectively
        - *'30'* stands for the number of intervals to take while scanning through theta within the given range
        - *'-10'* stands for the number of accumulations to make at each frame (the minus sign is there as a convention)
    b. Using the *'ascan'* function where the function is used as follows:
        - *'ascan th -0.25 1 30 -10'*
        - The *'th'* lets the system know that we want to vary theta
        - *'-0.25'* and *'1'* are the initial and final values of the theta range respectively
        - *'30'* stands for the number of intervals to take while scanning through theta within the given range
        - *'-10'* stands for the number of accumulations to make at each frame (the minus sign is there as a convention)
3) Once the scan is initiated, the options in the scanning software, WinView, need to be adjusted accordingly. The number of accumulations, exposure time and the number of frames are all entered here. Number of accumulations is equal to the number entered in the 'lup' or 'ascan' function, while the number of frames is the number of intervals plus one (in the example shown here, there are 31 frames). The exposure time is determined by techniques discussed earlier.
4) The progress of the scan may be seen on the terminal window, while the diffraction pattern may also be observed during the scan on WinView.

The process described herein is carried out at different places on the sample where interesting diffraction patterns are seen. The same experiments were carried out on another Indium Phosphide sample (InP #5) but this sample did not yield sufficient results.

2.3.6 Reconstruction

As the diffraction data is in reciprocal space, the data needs to be inverted back to real space to obtain an image of the nanowires. This is achieved via two separate algorithms namely, Error Reduction and Hybrid Input Output. Both algorithms are similar as they are both iterative algorithms yet different in approach.

Let an object in real space be **f(x)** and its reciprocal space counterpart (Fourier Transform of **f(x)**) be **F(u).** As **F(u)**, as well as **f(x)**, is a vector, it can be split into its real and imaginary components, amplitude and phase respectively, as follows:

$$F(u) = |F(u)|e^{i\psi(u)} = \mathfrak{F}\{f(x)\} \equiv \int\int_{-\infty}^{\infty} f(x)\, e^{-i2\pi u \cdot x} dx \qquad (2.1)^{13}$$

where $\mathfrak{F}\{f(x)\}$ stands for Fourier transform of $f(x)$

During the diffraction experiments, it is the amplitude of this Fourier function that is measured and hence the phase information is lost. To recover this phasing information, we make use of the algorithms mentioned previously.

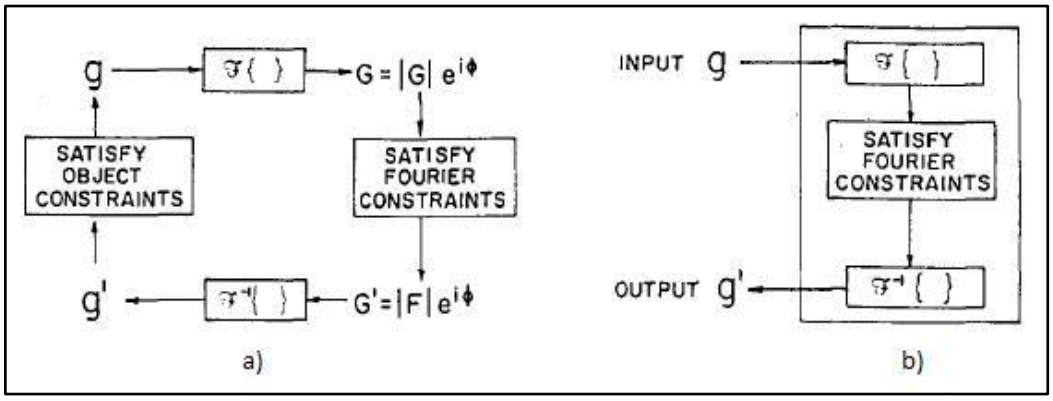

Figure 2.16: a) Block diagram of the Error Reduction (ER) algorithm; b) block diagram of the system for the Hybrid Input-Output (HIO) algorithm[13]

The Error Reduction algorithm works by an iterative approach (see Figure 2.16 (a)) as shown by the following steps:

1) Begin with a random estimate of the object, g, in real space
2) The real space object, g, is Fourier transformed to obtain the corresponding diffraction pattern, $G = |G|e^{i\emptyset}$, in reciprocal space
3) As the value of the moduli, $|F|$, in reciprocal space is available from our *experimental* diffraction pattern, the *iterative* diffraction pattern, G, is made to conform to this constraint to give $G' = |F|e^{i\emptyset}$
4) The new *iterative* diffraction pattern, G', is inverse-Fourier transformed to obtain a new estimate of the object, g', in real space
5) Object constraints are applied to the new estimate of the object, g', namely that the object be non-negative and also *'zero outside the known boundary of the object (the support)'*:

$$g_{k+1}(x) = \begin{cases} g_k', & x \notin \gamma \\ 0, & x \in \gamma \end{cases} \quad (2.2)^{13}$$

where g_{k+1} is the $(k+1)th$ iteration of the real space object, g

γ contains all the points where g' violates the object constraints

Hence if a particular point does not violate the object constraints, the value is unchanged and fed back as the input for the next iteration. Whereas if the object constraints are violated by a particular point then the value of that point is turned to zero.

6) The new estimate of the real space object is iterated beginning from step 1 until a sufficient solution is found

A measure of the error in the iterative object is the chi-squared value (also known as residual value or mean-squared error). This is calculated as follows:

$$\chi^2 = \frac{\sum(A^{calc} - A^{meas})^2}{\sum(A^{meas})^2} \quad (2.3)$$

where A^{calc} is the iteratively calculated amplitude of the diffraction pattern

A^{meas} is the experimentally measured amplitude of the diffraction pattern

Due to the manner in which the Error Reduction algorithm operates, the chi-squared value, and hence the error in the calculated object, decreases with each iteration of the algorithm. There is a large decrease in the chi-squared value at first but this becomes very small after a few iterations.

The other vital algorithm used in the reconstruction of the object is called the Hybrid Input Output (HIO) algorithm (see Figure 2.16 (b)). The HIO algorithm is exactly the same as the Error Reduction algorithm up until where the object constraints are applied to the new estimate of the object, g'. Instead, g' is used to generate a new input to the algorithm using the following relationship:

$$g_{k+1}(x) = \begin{cases} g_k(x), & x \notin \gamma \\ g_k(x) - \beta g_k'(x), & x \in \gamma \end{cases} \quad (2.4)^{13}$$

where β is known as the feedback parameter

γ contains all the points where g' violates the object constraints

Hence if a particular point does not violate the object constraints, it is unchanged in the new input. On the other hand, if a particular point does violate the object

constraints, then the value at that point is multiplied by the feedback parameter, β, and the result is subtracted from the initial value at that point. This method is much quicker in reaching a constant chi-squared value, although experiments show that it works best when used in conjunction with the Error Reduction algorithm[13].

A support, in its simplest form, a cuboid, is also required for both algorithms. The real space object is defined only within this support; hence it is vital to have the right-sized support. The Error Reduction algorithm turns all points outside of the support to zero after each iteration, while the Hybrid Input Output algorithm attempts to bring these points inside the support by changing their values.

As both algorithms are generally run together in a sequence of ER-HIO-ER, a small-sized support will cut through the object with half of it being inside the support and half outside. Due to the Error Reduction algorithm being run last in the iterations, the amplitude of the points outside of the support will be turned to zero, which means only the part of the of the object within the support is visible. A large-sized support, on the other hand, allows many different solutions to the object, be possible and hence raises the chi-squared value considerably as the error in the solution is great.

The reconstruction process begins by firstly adjusting the diffraction pattern, which is contained within a .SPE file using WinView. Firstly, the .SPE file is cropped to exclude any unwanted noise and any possible 'aliens' floating around near the nanowire of concern. The term 'alien' is given to any significant diffraction pattern, which cannot be considered as simple noise but is a pattern that is not related to the main diffraction pattern of concern. It is necessary to have a pure diffraction pattern when reconstructing the nanowire as the 'aliens' and significant noise will either decrease the resolution of the solution or add extra unwanted features to the solution. Although, some 'aliens' are such that they cannot be cropped out as that would mean cropping part of the main diffraction pattern as well. This narrows down the useful nanowires from the not so useful ones greatly. An example of such a case is shown in Figure 2.17, where the 'aliens' are circled for clarity.

The diffraction pattern is now binned, where binning is the process whereby adjacent pixels are combined to give one pixel. For example, if an array size of 60 × 60 pixels was binned 2 × 2, then the resulting array size would be 30 × 30 pixels; if it was binned 3 × 2, then the resulting array size would be 20 x 30 pixels. The process of binning can be performed before the readings are taken and also after the readings are taken.

The advantage of binning before performing the theta scan is that it can minimise the random noise recorded. A CCD consists of an array of pixels whereby photons are counted. For example, consider a CCD with 2 × 2 pixels:

- No binning (1 x 1): Photons would be counted individually for each of the four pixels and random noise would be recorded for each pixel as well
- Binning (2 × 2): The same number of photons would still be counted but as effectively only one pixel is taking the readings, the random noise is only recorded once and hence there is a larger signal to noise ratio

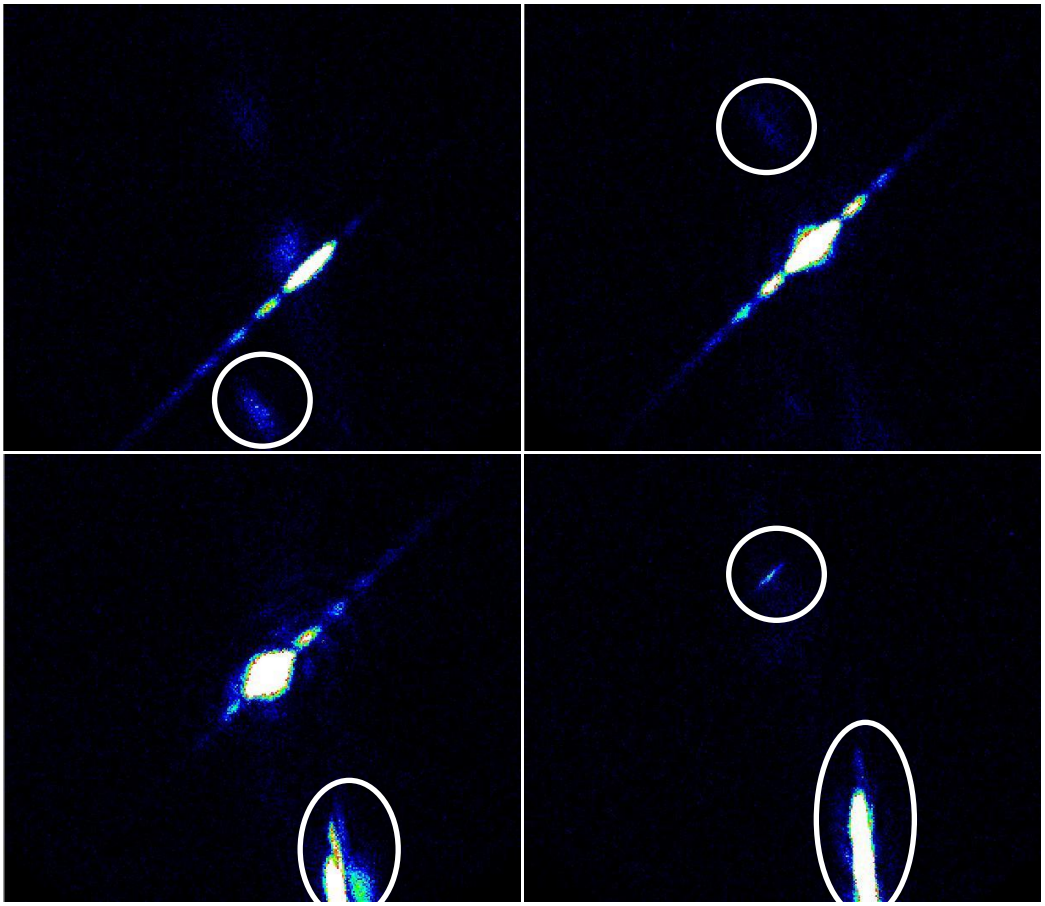

Figure 2.17: Diffraction pattern of a typical nanowire shown at frame = 22 (top left), 34 (top right), 49 (bottom left) and 63 (bottom right) – 'Aliens' are circled[14]

The advantage of binning after the theta scan has been performed is that you do not lose any resolution due to binning beforehand and also it reduces the file size and hence the amount of time each nanowire takes while running the iterative algorithms. If binning is carried out after the theta scan has been performed then the amount of binning required is determined by having at least a few pixels spacing between the fringes of the diffraction pattern. Binning past this point results in the final solution losing resolution and hence losing essential features.

The next step is to collect all the relevant information required to start the iterative algorithms. Table 2.2 lists all the parameters required for the process of reconstruction. While some of the parameters are experiment-dependant, some are constant throughout, including the wavelength of the x-ray beam and the detector arm length. As all diffractometer motor positions are recorded in a .SPC file, a few parameters required herein are obtained using software capable of displaying the data of .SPC files, namely this software is Newplot.

Parameter	How to determine it
Array Size	Found in WinView
Centre of diffraction pattern	Most intense pixel of the diffraction pattern – intensity of each pixel is specified in WinView
Buffer Array	Usually chosen to be approximately 25% larger than the Array Size
Feedback parameter, β, for HIO algorithm	Chosen to be β = 0.9
Number of iterations for each algorithm	Usually chosen to be 20 iterations of Error Reduction algorithm followed by 50 iterations of HIO algorithm and finally 20 iterations of Error Reduction Algorithm
Phase constraints for HIO algorithm	Phase chosen to be constrained within $-\frac{\pi}{2}$ and $+\frac{\pi}{2}$
Detector arm length	Measured manually before performing the diffraction experiments (arm length = 0.871 m)
Wavelength of x-ray beam	The energy of the beam is displayed on the electronics rack outside the Coherent Diffraction Hutch. Using Planck's relationship of energy and wavelength, the wavelength can be determined: $$E = \frac{hc}{\lambda}$$ where E = energy, h = Planck's constant, c = speed of light in vacuum and λ = wavelength
Detector angles: delta and gamma	All diffractometer motor positions are recorded for each experiment in a single .SPC (specification) file (viewed using Newplot) whereby the angles are found
Binning	The total amount of binning done both, before and after the theta scan (e.g. A binning of 2 × 3 before and a binning of 2 × 2 after the theta scan results in a total binning of 4 × 6)
Step values of theta	$$\frac{Total\ range\ of\ the\ theta\ scan}{Number\ of\ intervals}$$
Support size	Arbitrarily chosen at first and adjusted after each attempt at the reconstruction. A good initial support size is +/- 25 in all three directions (x, y and z)

Table 2.2: List of parameters required for the reconstruction process along with how to obtain the values

The above parameters are fed into several scripts which in turn run the Error Reduction and HIO algorithms and hence produce a real space 3D image of the result. The full library of scripts has been written by Garth J. Williams and Mark A. Pfeifer, while being continuously edited by Steven Leake, Ross Harder and Ian K. Robinson.

Chapter 3: Results

- Diffraction data – a few images showing the different kind of results gained from the runs and the parameters used for each example

Chapter 4: Analysis

- Method of how to reconstruct? (not sure whether to put this as part of the experimental methods section or at the beginning of the analysis section)
- Reconstructed nanowire images
- Sizes of nanowires seen
- Phase maps to show there is strain (2pi phase parallel to Q vector = 1 lattice constant of displacement? Not sure which direction expansion/compression are…)
- Some statistics about the random starts and how a ‘coffin’ support results in a non-symmetric solution 50 out of 50 times
- Ribbing is an artifact of random starts? (need to confirm this still)

Chapter 5: Conclusion

- CXD used to image nanowires
- Diffraction data is reconstructed using ER and HIO algorithms
- Strain can be seen on nanowires
- Future things to do – rotate the support, analyse more diffraction data, study strain in more detail

References

[1] http://www.sca.asn.au/nletters/sca42.htm - Society of Crystallographers

[2] C. Benson and I. K. Robinson, Synchrotron Radiation Instrumentation: Eleventh US National Conference **521** 230-233 (Jun 2000)

[3] University of Ilinois at Urbana-Champaign and Oak Ridge National Laboratory, 'Final Design Report for UNICAT Beamline Sector 34 at the Advanced Photon Source at Argonne National Laboratory' (Oct 2000)

[4] University of Ilinois at Urbana-Champaign and Oak Ridge National Laboratory, 'Preliminary Design Report for UNICAT Beamline Sector 34 at the Advanced Photon Source at Argonne National Laboratory' (Sep 1998)

[5] A. Nadkarni, P. K. Samal, J. E. Synk, US Patent No: 4999336, 'Dispersion strengthened metal composites' (Mar 1991)

[6] D. Shu, B, Rodricks, J. Barraza, T. Sanchez, and T. M. Kuzay, Nuclear Instruments & Methods in Physics Research, Section A **319** 56-62 (1992)

[7] http://www.aps.anl.gov/APS_Engineering_Support_Division/User_ESH/Reference/Shutters/ - P9 Photon Shutters

[8] P. K. Job, Advanced Photon Source Technical Bulletins, 'Guidelines for Beamline and Front-End Radiation Shielding Design at the Advanced Photon Source' **ANL/APS/TB-44 Rev. 2** (May 2005)

[9] M. Newville, Denver X-ray Conference, 'Kirkpatrick-Baez Focusing Mirrors' (Jul 2001)

[10] P. Kirkpatrick and A. V. Baez, Journal of the Optical Society of America, **38** 766-774 (Sep 1948)

[11] http://www.seas.ucla.edu/ms/faculty1/S_Kodambaka.htm

[12] Private communication with Robyn Woo by e-mail

[13] J. R. Fienup, Optics Letters, 'Reconstruction of an object from the modulus of its Fourier transform', **3** 27-29 (Jul 1978)

[14] Filename of the diffraction pattern: NW408-106.SPE